Journal of Physics:
Conference Series

PURPOSE-LED
PUBLISHING™

PAPER • OPEN ACCESS

Heat Transfer Equipment for a Compressed Air Energy Storage (CAES) Integrated with a Concentrated Solar System

To cite this article: Jacopo Romani *et al* 2025 *J. Phys.: Conf. Ser.* **3143** 012061

View the article online for updates and enhancements.

You may also like

- Study of the effects of heat-treatment of hydroxyapatite synthesized in gelatin matrix
A V Zaits, O A Golovanova and M V Kuimova
- Comparative performance of machine learning models for the classification of human gait
Divya Thakur and Praveen Lalwani
- Triangular and Octagonal Array Grammars
S. Kuberal, K. Bhuvaneswari and T. Kalyani

This content was downloaded from IP address 109.112.160.84 on 03/02/2026 at 14:56

Heat Transfer Equipment for a Compressed Air Energy Storage (CAES) Integrated with a Concentrated Solar System

Jacopo Romani[1a], Coriolano Salvini[1],

Ambra Giovannelli[1], Erika Maria Archilei[1], Gianluca Cevolani[1]

[1]Department of Industrial, Electronic and Mechanical Engineering, University of ROMA TRE, Via della Vasca Navale 79, ROMA.

[a)] Corresponding Author: Jacopo Romani (jacopo.romani@uniroma3.it)

Abstract. The transition to sustainable electric grids requires advanced solutions to address the intermittency of renewable energy sources. The integration of a Compressed Air Energy Storage (CAES)with a Concentrated Solar Power Plant (CSPP) constitutes a promising solution to develop high-efficiency and zero-emission plants. In the proposed concept, the concentrated solar radiation is absorbed and stored in a High-Temperature Thermal Energy Storage (HTES) at 800 °C. During the CAES discharge phase, air at a nearly atmospheric pressure is used as thermal carrier to heat the stored compressed air before the expansion in a High-Pressure Turbine (HPT) and to reheat the HPT exhaust air before the expansion in a Low-Pressure Turbine (LPT). Medium/large CAES plants (20-100 MWe) are addressed. Therefore, to make the heat exchangers compact, conventional configurations like Shell&Tube (S&T) arrangements could be replaced by unconventional ones. One option is the adoption of the consolidated industrial Heat Recovery Steam Generator (HRSG) technology to design a Hot Air Generator (HAG). According to such a concept, the HAG is made of tube bundles placed into a rectangular duct. Such a configuration allows the installation of large heat exchange surfaces, making the HAG performance higher than S&T HT ones. In the present paper, preliminary design studies of a HAG for a 20 MWe CAES plant have been carried out. A computational code focused on HAG design has been developed in Visual Basic for Application (VBA). Different design layouts are presented and discussed. Finally, HAG off-design performance is shown in the entire expected operating range.

INTRODUCTION

Proactive integration strategies are needed to fully exploit the expansion potential of solar PV and wind power [1]. In the last few decades, to support the energy transition electric grids have integrated power production from non-programmable renewable sources. The high penetration of such sources has led to a significant reduction of GHG emissions [2].

However, power generation from PVs and wind farms is intermittent and poses several issues in terms of power grid management, reliability and stability. To overcome such concerns, it is mandatory to make the grid more flexible, for instance by increasing energy storage capacity. Energy storage can mitigate the phenomena associated with the intermittency of energy supply and demand [3]. There are several technologies for storage systems such as electrochemical, mechanical, chemical, electrical and thermal [4] [5]. Among them, a suitable solution for utility-scale applications are mechanical ones such as Pumped Hydro Energy Storage (PHES), Liquid Air Energy Storage (LAES) and Compressed Air Energy Storage (CAES). PHES is undoubtedly the most mature technology for large capacity energy storage systems [2]. It is characterised by high round-trip efficiencies (RTE) and long operating life, but it is strongly constrained by orographic availability. LAES, although having high potentials, has great complexity and, consequently, a high CAPEX [6]. CAES systems, thanks to the high operating

Content from this work may be used under the terms of the Creative Commons Attribution 4.0 licence. Any further distribution of this work must maintain attribution to the author(s) and the title of the work, journal citation and DOI.
Published under licence by IOP Publishing Ltd

life, low environmental impact, high reliability, synchronous inertia and economic feasibility [7], [8] and [9], are promising solutions and, therefore, are considered in this paper.
In CAES plants, surplus electricity is used to drive a train of compressors able to store pressurised air in a natural or artificial reservoir. During periods of high demand, the pressurised air is forced to expand through a series of turbines after adequate air heating. Existing plants such as Huntorf and McIntosh are so-called diabatic CAES (D-CAES). In these plants, the pressurised air is heated during the discharge phase entirely or partially by an external heat source like fossil fuels or exhaust gas from a gas turbine engine [10], [11], [12]. This results in GHG emissions during the discharge phase and in the achievement of limited efficiency. To overcome these issues, hydrogen produced from electricity generated by renewable energy sources can be used. In this case, important design aspects related to the use of non-conventional fuel must be properly addressed, as reported in [13].

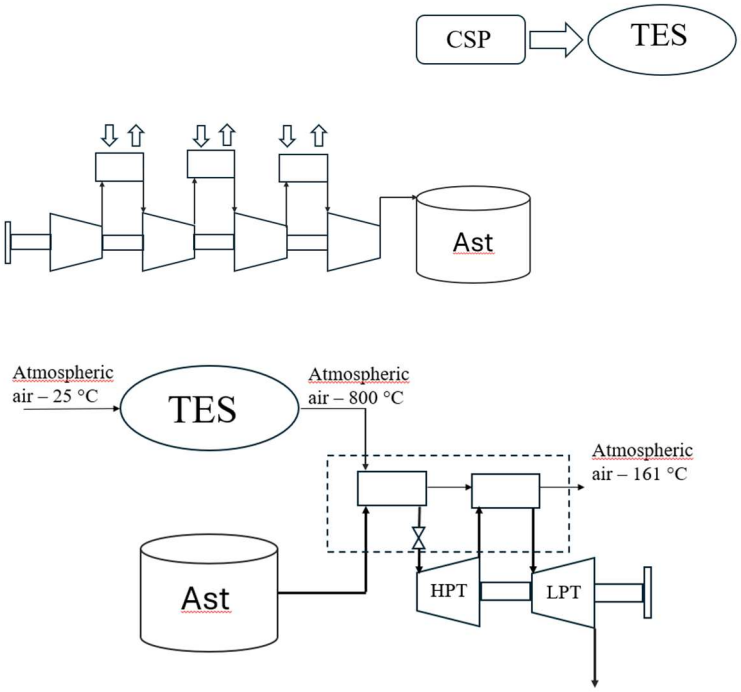

Figure 1. Charging and discharging phase plant layouts

To avoid CO2 emissions and increase the system efficiency, an alternative strategy is to replace the combustion chamber with a solar-based heat generation unit. By integrating a CSP with a CAES system, it is possible to increase the air temperature at the inlet section of the turbines avoiding the aforementioned design issues. The integration between a CSP and a CAES is proposed and analyzed in [14] and [15]. In the present study, a 20 MWel plant layout proposed and developed in the EU funded research project ASTERIx&CAESar [16] is assumed as a reference (Fig. 1). During the charging phase, pressurized air is stored in an Air Storage Tank (AST), while the CSP allows heat storage at high temperature in a Thermal Energy Storage (TES). During the discharge phase, when electricity demand is high, an air stream at nearly atmospheric pressure is used to remove the thermal energy from TES. Such a stream is then sent to a high temperature heat transfer plant section to heat and re-heat the pressurized air

before the expansion in High Pressure Turbine (HPT) and Low-Pressure Turbine (LPT) respectively, as shown in the lower part of Fig.1.
The paper focuses on the design of the high temperature heat transfer section. An unconventional approach based on the consolidated industrial Heat Recovery Steam Generator (HRSG) technology is proposed to design a Hot Air Generator (HAG) capable of heating and re-heating the pressurized air.
Basically, a HRSG is constituted by a rectangular duct containing the required number of tube bundles. Water or steam flow inside the tubes, while the Gas Turbine exhaust gas flows externally.
In the present application, water/steam on tube side is replaced by pressurized air. Interesting aspects are related to the reduced duct side pressure losses, the possibility of using externally finned tubes, the capability of managing relevant heat duties and large atmospheric air volumetric flow rates.
The aim of this paper is to analyze and discuss different HAG arrangements. A computational code focused on HAG design has been developed in Visual Basic for Application (VBA). Different design layouts are presented and discussed. Finally, HAG off-design performance is shown in the entire expected operating range.

1. Preliminary component analysis

To simulate the operation of the aforementioned heat exchanger, a preliminary analysis is performed using CHEMCAD 7 software.
After numerous simulations, the final adopted configuration is constituted by four bundles, two of them in parallel as shown in Figure 2.

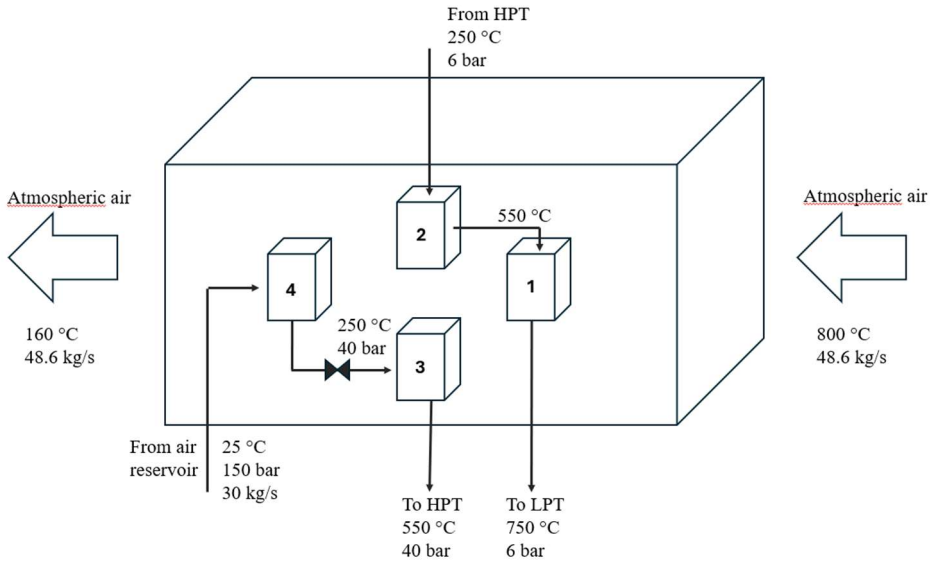

Figure 2. Schematic representation of the device

The figure highlights that the HAG consists of a first bundle with high temperature and pressurised air in the tubes. The pressurised air leaving this tube bundle feeds the low-pressure turbine (LPT). The two parallel tube bundles are crossed with atmospheric air from the outlet of first bundle; the pressurised air on the tube side flows into low pressure (6 bar) preheater and

into a medium pressure bundle at approximately 40 bar that feeds the high-pressure turbine (HPT).

The last bundle is used to preheat the air leaving the air reservoir at high pressure (up to 150 bar). The system operates at constant mass flow rate. A constant pressure is maintained at the HPT inlet by a pressure control valve.

The results (reported in Table 1) achieved using CHEMCAD 7 are the input data for the preliminary design of the HAG.

N° of bundle	**#1**	**#2**	**#3**	**#4**
Mass flow rate (duct side) [kg/s]	48.6	24.2	24.2	48.6
Mass flow rate (tube side) [kg/s]	30.0	30.0	30.0	30.0
Tubes: Inlet/Outlet temperature [°C]	550 /750	250/550	250/550	25/250
Duct: Inlet/Outlet temperature [°C]	800/678	678/314	678/312	313/160
Tube/Duct pressure [bar]	6/1	6/1	40/1	150/1

Table 1. Input data

A specific in-house code was written in VBA language for designing suitable device configurations. In particular, the Logarithmic Mean Temperature Difference (LMTD) method was adopted for the calculation of global heat transfer surface. Unlike combustion gases in HRSGs, in this application there are no triatomic gases that can make a noticeable contribution to heat exchange by radiation. Therefore, the only heat exchange mechanism considered is by convection.

2.Design

Starting with the input data, the VBA code allows the design of tube bundles consituting the HAG. The code works in accordance with the flowchart shown in Figure 3. A description of the calculation procedure is given in the following.

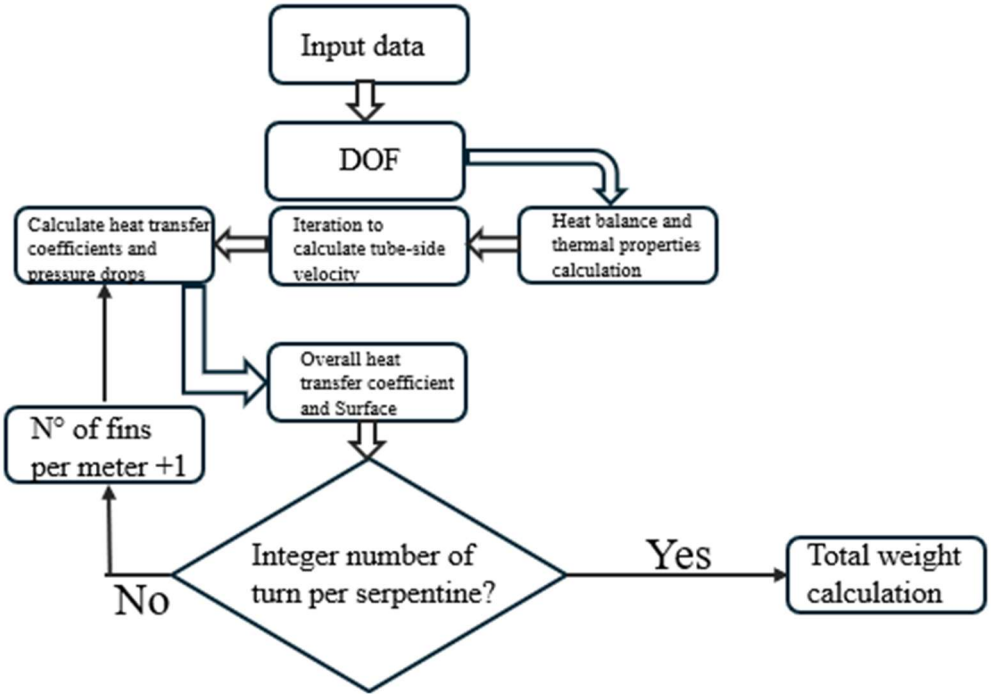

Figure 3. Flow chart for the program

2.1 Degrees of freedom and constraints

Degrees of freedom (DOF) are quantities chosen by the designer necessary to completely define the design for each tube bundle. Common degrees of freedom for the two designs addresses in the following were selected after an extensive preliminary calculation campaign.
By imposing a certain passage velocity, taken by analogy with the values of the free-section velocity of the combustion gases in HRSGs, and choosing an appropriate height-to-width ratio of the duct, the values of duct height and width are derived. Further DOF are the pipe diameter, thickness, type of pipe, type of arrangement, the ratio of longitudinal to transverse pitch over tube diameter, type of fin, fin pitch, diameter and thickness of fins, and the choice of material from which the different tube bundles are made. Values selected for each tube bundle are reported in Table 2.
The constraints adopted for the design of the various tube bundles are related to the maximum tube-side velocity and pressure drop on the duct side.

2.2 Design procedure

The in-house tool developed *ad hoc* for the design is based on iterative procedure to obtain an integer number of tubes.
Inputs, DOFs, and constraints are provided through excel sheets. The tool relates to NIST REFPROP v. 10.0 libraries for the accurate evaluation of the working fluids thermodynamic properties (e.g. density, thermal conductivity, viscosity, enthalpy, and Prandtl number). The duct size and, consequently, the number of tubes that can be placed in the first row are initially evaluated.

N° of bundle	**#1**	**#2**	**#3**	**#4**
Free flow velocity [m/s]	6	5.29	5.29	3.27
Duct height/width ratio	1	2	2	1
Tube diameter [m]	0.073	0.0603	0.0422	0.0483
Tube thickness [m]	0.00515	0.00318	0.00485	0.00714
Tube arrangement [Inline, Staggered]	Inline	Inline	Inline	Inline
Tube type [Bare, Finned]	Bare	Finned	Finned	Finned
Transversal pitch to diameter ratio	1.25	1.33	1.45	1.4
Longitudinal pitch to diameter ratio	1.25	1.33	1.85	1.49
Fins type [Solid, Serrated]	-	Solid	Solid	Solid
Fins height [m]	0.008	0.008	0.008	0.008
Material	Alloy 625	SS 347	SS 347	C45

Table 2. Degree of Freedom (DOF)

Then, the number of parallel rows is evaluated under the constraint of the maximum allowable pipe-side velocity. The process is iterative, and an additional parallel path is added whenever the calculated velocity exceeds the allowable velocity. The Dittus-Boelter (tube-side) and Babcock & Wilcox (duct-side) relationships are used [17], [18] to evaluate the overall heat transfer coefficient.

The overall heat transfer coefficient and the total exchange surface area are calculated. For finned tubes, a specific procedure given in [17], is followed to calculate the heat transfer coefficient on the external side of tubes [19].

To achieve an integer number of parallel passes, the number of fins per meter varies iteratively until an integer number of passes is obtained with a tolerance of 3%. By changing the initial boundary conditions (i.e., the starting fin pitch) different arrangements of the tube bundles are obtained. In this way, among the various solutions achieved, it is possible to select those ones characterized by the minimum amount of metal and therefore, presumably, the lowest costs. In parallel with the procedure for calculating the overall heat transfer coefficient, the tube-side and duct-side pressure drops are derived. Regarding the latter, in the case of finned tubes, a procedure similar to the one adopted above for the calculation of the overall exchange coefficient is followed. A representation of the tube arrangement and fin type adopted is shown in Figure 4 in Appendix 2. The most relevant relationships adopted are reported in detail in Appendix 2 also. The code has been succesfully validated against a real tube bundle. Details are given in Appendix 1.

3 Results and discussion

Simulations are carried out for two different air heater design configurations called in the following Design 1 and Design 2. In the first one, the design is aimed at reducing tube side pressure losses in each individual tube bundle. Therefore, the maximum tube side velocity is limited to 20 m/s.

N° of bundles	Tubes per row x parallel serpentines	N° of turns per serpentine	N° tubes	Tube type	Nalm	Tube pitch [m]	S'	U'	Weight [ton]
#1	51 x 5	6	1530	Bare	0	0.091	1756	46.3	70.9
#2	28 x 10	6	1680	Finned	42	0.080	2832	36.9	47.8
#3	38 x 3	8	912	Finned	124	0.061	2091	50.2	32.1
#4	71 x 1	8	568	Finned	167	0.067	1824	44.1	31.2

Table 3. Results of design 1, S'= total heat transfer surface [m^2], U'= total heat transfer coefficient [$W/(m^2K)$], Nalm= number of fins per meter

In Design 2, the weight reduction was privileged by limiting the total number of tubes. Therefore, to enhance the overall heat transfer coefficient, a higher value of tube side velocity of 25 m/s has been assumed.

N° of bundles	Tubes per row x parallel serpentines	N° of turns per serpentine	N° tubes	Tube type	Nalm	Tube pitch [m]	S'	U'	Weight [ton]
#1	51 x 4	7	1428	Bare	0	0.091	1641	49.3	54.3
#2	28 x 8	6	1344	Finned	78	0.080	3131	33.3	45.0
#3	38 x 2	10	760	Finned	164	0.061	2142	49.1	29.8
#4	71 x 1	8	568	Finned	167	0.067	1824	44.1	31.2

Table 4. Result of design 2, S'= total heat transfer surface [m^2], U'=total heat transfer coefficient [$W/(m^2K)$], Nalm= number of fins per meter

Results achieved for Design1 and Design 2 are given in Tables 3 and 4, respectively.
To facilitate comparison between the two solutions, Table 5 shows the values of the notable quantities for the two solutions. Some relevant aspects are discussed in the following.

	Unit	Design 1	Design 2
Tube number		4690	4100
Total surface	m^2	8503	8738
Bundle n° 1	ton	70.9	54.3
Bundle n° 2	ton	47.8	45.0
Bundle n° 3	ton	32.1	29.8
Bundle n° 4	ton	31.2	31.2
Total weight	ton	182.0	160.3
ΔP – 6 bar tube bundles	kPa	24.5	40.4
ΔP – 40 bar tube bundle	kPa	184.3	508.0
ΔP – 150 bar tube bundle	kPa	65.1	65.1
ΔP duct	kPa	2.25	2.24
Duct lenght	m	8.1	7.0

Table 5. Comparison between design n°1 and n°2

- On the basis of the results reported in Table 5, Design 2 reduces of 13% the tubes number in respect to Design 1. As a consequence, Design 2 shows a weight of 160 tons against 182 tons of Design1. The first tube bundle is without fins since there is no particular benefit in adopting extended surface, as the heat transfer coefficients on internal and external tube sides are in the same order of magnitude. Furthermore, in industrial HRSG, there are no finned tube bundles operating above 600 °C.
- As expected, a relevant difference between the two designs is achieved in terms of tube side pressure losses. Such a difference is due to the higher allowable tube side velocity assumed in Design 2. Tube side pressure drops are related to the work produced in the expansion train. As shown in Figure 2, the pressure at HPT inlet is maintained constant by the control system. Therefore, the work reduction is related to pressure losses in bundles n°1 and n°2. As reported in Table 5, pressure drops of 24.5 and 40.4 kPa are calculated for Design 1 and Design 2, respectively.
- Duct side pressure drops increases with the number of tube rows crossed by atmospheric air and with the fin pitch (eq. 4 in Appendix 1). It can be noticed as Design 1 is characterized by a higher number of tube rows in respect to Design 2. Conversely, the tube bundle of Design 1 has a lower number of fins per meter than Design 2. As a result, the pressure drop is pratically the same for the two design solutions. Therefore, the same amount of power is requested to circulate the atmospheric air mass flow rate.
- The above results indicate economic implications for different design solutions. A design with fewer tubes implies lower weight and, therefore, a lower cost of the tube

bundle associated with the reduced quantity of metal used. Fewer tubes also mean fewer machining operations, resulting in further economic savings. According to [20], the capital cost was associated with the weight. The cost was taken equal to 7 USD/kg and 10 USD/kg for carbon and alloy steel materials, respectively. Such figures are appllicable to bundles n° 2 and n° 3 (made of stainless steel S.S.347 as reported in Table 2), and tube bundle n°4 (made of carbon steel C45). To withstand the really high design temperatures, Alloy 625 (a Cr-Ni Alloy) was selected for tube bundle n° 1. The cost of Alloy 625 was set equal to 4 times the cost of S.S. 347, as suggested in [21]. Therefore, the cost of bundle n° 1 has been estimated by assuming a material cost of USD 40/kg. In conclusion the costs for Design 1 and Design 2 are about 3,800,000 and 3,100,000 USD, respectively.

- Finally, a simple off-design analysis was performed by using CHEMCAD software. A constant mass flow rate discharge phase has been assumed according to ASTERix-CAESar project specification [22]. The atmospheric air temperature entering the HAG is supposed to decrease during discharge phase from 800 to 750 °C. The HAG behaviour at the end of the discharge phase has been checked. Results are given in Table 6. The variation of heat transfer coefficients in respect to design conditions is essentially related to changes in duct side and tube side mass flow rates. Since both mass flow rates remain constant and a reduced variation of the atmospheric air inlet temperature is considered, design values of the overall heat transfer coefficients are assumed for all tube bundles. It can be noticed that the temperature at LPT inlet varies by 6% from the design condition, while the inlet temperature at HPT varies by 5.5%. Assuming expansion up to 1 bar and a polytropic efficiency of 0.85, specific work reductions of about 5% in LPT and 4% in HPT are estimated.

Temperature	Unit	Design	Off - design
T_{atm}.in.	°C	800	750
T_{in} LPT	°C	750	705
T_{in} HPT	°C	550	520
Tdisch	°C	161	155

Table 6. Off-design results. T_{atm} in = temperature of atmospheric air at the inlet, T_{in} LPT=inlet LPT temperature, T_{in}HPT=inlet HPT temperature, Tdisch=temperature of atmospheric air at the outlet.

4 Conclusion

The purpose of this paper is to design a heat exchange equipment based on industrial HRSG technology that can be used in an integrated CSP-CAES system. A plant size of 20 MWel has been taken as reference. The results can be summarised as follows:

- Values of overall heat transfer coefficients typical of an HRSG have been found.
- The weight of each tube bundle decreases as the fin pitch increases. Moreover, the advantage in adopting fins is more significant when the tube side and duct side heat transfer coefficients significantly differ. This occurs in tube bundles operating at 40 and 150 bar (tube bundles n° 3 and n° 4) which are typical pressure values found in HRSG. The tube-side and duct-side heat transfer coefficients differ very slightly in the first tube bundle, which is why it was decided to adopt a bare tube solution.

- Design 2 is preferable from the point of view of lower equipment weight. However, this system results in higher pressure drops that could impact plant savings. Conversely, Design 1 is preferable from the point of view of lower pressure drop. However, this implies a greater weight of the device.
- The HAG off design behaviour has been succesfully checked.
- In conclusion, the proposed approach based on HRSG technology seems succesfully applicable in CSP-CAES integrated plants.

Acknowledgements

This work has received funding from the European Union's Horizon Europe research and innovation program under project "ASTERIx&CAESar" with grant agreement Nº 101122231. This research was conducted with fundamental support of the "ASTERix&CAESar" Project Team. The Authors would like to thank the Department of Industrial, Electronic and Mechanical Engineering, University of ROMA TRE for providing access to essential resources.

Appendix 1

To validate the in-house developed tool, the design of a real existing superheater bundle whose data are given in [20] was carried out. Design input data are reported in Table 7. It can be noticed that really good agreement between calculated and real data is achieved, as shown in Table 8.

Input data	**Unit**	
Tube arrangement		Staggered
Tube diameter	mm	38,1
Transversal pitch	mm	96
Longitudinal pitch	mm	90
Fin type	Solid	Solid
Fin height	mm	10
Fin thickness	mm	1.2
Lenght of fin tube	m	15.7

Table 7. Input data used for the validation

Calculated data	**Unit**	**Existing superheater**	**Calculated with VBA code**	**delta %**
Number of rows		3	3	
Tubes per row		78	78	
Nalm		120	120	
U'	$W/m^2 K$	61.8	61.0	-1.3
S'	m^2	1805.4	1843.5	2.1
Flue gas pressure drop / p_{in}	%	0.079	0.072	---

Table 8. Data derived from the code, S'= total heat transfer surface [m2], U'=total heat transfer coefficient [W/(m2K)], Nalm= number of fins per meter

Appendix 2

The most relevant equation used in the program are shown below. It is also reported a simple scheme of the arrangment and the type of fin adopted in both designs

$$U_{finned} = 1 / (((1 / \alpha) (So / (ef\ Sf + Sb))) + ((s\ So) / (\lambda_m\ Sm)) + ((1 / \alpha_t) (So / Si))) \quad (1)$$

$$U_{bare} = 1 / ((1 / \alpha) + ((s / \lambda_m) (de / dm)) + ((1 / \alpha_t) (de / di))) \quad (2)$$

$$S = (Q_1 / (\Delta T_{ml}\ U)) \quad (3)$$

$$\Delta p_{finned} = 0.02(f + a) (m_1 / Amingfin)^2\ n_p\ N_{fp} / \rho) \quad (4)$$

$$\Delta p_{bare} = 1.83\ f_a\ f_d\ n_0\ N_{fp}\ (T / 1000)\ ((m_1 / Aming)^2)\ (1 / \rho_0) \quad (5)$$

$$\Delta p_t = \rho_{21}\ (ct_1^2)\ 0.5\ f\ leq\ (1 / di)\ N_{fp}) \quad (6)$$

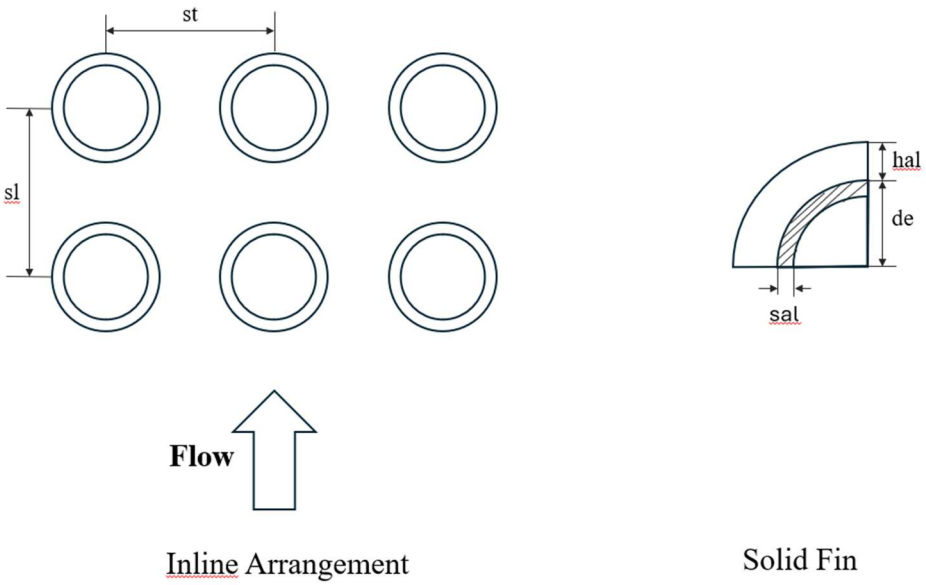

Figure 4. Tube arrangement and fin type adopted, sl=longitudinal pitch, st=transversal pitch, de=external tube diameter, sal=fin thickness, hal=fin height.

Nomenclature

a=coefficient
α= heat transfer coefficient on duct side
α_t= heat transfer coefficient on duct side
Amingfin= cross section
ct_1= tube velocity
de= external diameter
di= internal diameter
dm= mean diameter
Δp= duct side pressure drops
Δp_t= tube side pressure drops
ΔT_{ml}= logarithmic mean temperature difference
ef= fins efficiency

ΔT_{ml}= logarithmic mean temperature difference
f= coefficient

f_a = arrangement factor

f_d =corrective factor = 1

Leq= equivalent lenght
λ_m= thermal conductivity
m_1= duct flow mass
N_{fp}= number of turns per serpentine
n_p= number of rows in parallel
Q_1= thermal power
ρ_0= density under normal conditions
ρ_{21}= inlet density
S= total heat transfer surface
s= tube thickness
ρ_{21}= inlet density

Sb= external tube surface not related to the fins for one meter tube lenght
Sf= fins surface for one meter tube lenght

Si= internal surface of the tube for one meter tube lenght
Sm= average surface for one meter tube lenght
So= S_f+S_b
U = overall heat transfer coefficient

References

[1] International Energy Agency , «Integrating Solar and Wind,» IEA, Paris, 2024.

[2] C. Salvini e A. Giovannelli, «Techno-Economic Comparison of Utility-Scale Compressed Air and Electro-Chemical Storage Systems,» *Energies,* vol. 15, n. 18, p. 6644, 2022.

[3] X. Luo, J. Wang, M. Dooner e J. Clarke, «Overview of current development in electrical energy storage technologies and the application potential in power system operation,» *Applied Energy,* vol. 137, pp. 511-516, 1 January 2015.

[4] H. Behabtu, M. Messagie, T. Coosemans, M. Berecibar, K. Anlay Fante, A. Kebede e J. A. Mierlo, «Review of Energy Storage Technologies' Application Potentials in Renewable Energy Sources Grid Integration,» *Sustainability,* vol. 12, p. 10511, 2020.

[5] A. A. Kebede, T. Kalogiannis, J. V. Mierlo e M. Berecibar, «A comprehensive review of stationary energy storage devices for large scale renewable energy sources grid integration,» *Renewable and Sustainable Energy Reviews,* vol. 159, p. 112213, 2022.

[6] A. Vecchi, Y. Li, Y. Ding, P. Mancarella e A. Sciacovelli, «Liquid air energy storage (LAES): A review on technology state-of-the-art, integration pathways and future perspectives,» *Advances in Applied Energy,* vol. 3, p. 100047, 25 August 2021.

[7] A. Olabi, T. Wilberforce, M. Ramadan, M. A. Abdelkareem e A. H. Alami, «Compressed air energy storage systems: Components and operating parameters – A review,» *Journal of Energy Storage,* vol. 34, p. 102000, 2021.

[8] G. Venkataramani, P. Parankusam, V. Ramalingam e J. Wang, «A review on compressed air energy storage – A pathway for smart grid and polygeneration,» *Renewable and Sustainable Energy Reviews,* vol. 62, pp. 895-907, September 2016.

[9] M. Budt, D. Wolf, R. Span e J. Yan, «A review on compressed air energy storage: Basic principles, past milestones and recent developments,» *Applied Energy,* vol. 170, pp. 250-268, May 2016.

[10] C. Salvini, «Performance assessment of a CAES system integrated into a gas-steam combined plant,» *Energy Procedia,* vol. 136, n. 8, pp. 264-269, 2017.

[11] C. Salvini, A. Giovannelli e D. Sabatello, «Analysis of diabatic compressed air energy storage systems with artificial reservoir using the levelized cost of storage method,» *International Journal of Energy Research,* vol. 45, pp. 254-268, 2021.

[12] A. G. Coriolano Salvini, «Techno-economic comparison of diabatic CAES with artificial air reservoir and battery energy storage systems,» *Energy Reports,* vol. 8, pp. 601-607, 2022.

[13] U. Gottipati, A. Minotti, V. La Battaglia e A. Giorgetti, «Design Challenges in the Development of a Hydrogen-Fueled Micro Gas Turbine Unit for Energy Generation,» *Engineering Proceedings,* vol. 85, n. 45, 2025.

[14] J. Baigorri, F. Zaversky e D. Astrain, «Massive grid-scale energy storage for next-generation concentrated solar power: A review of the potential emerging concepts,,» vol. 185, p. 113633, October 2023.

[15] F. Zaversky, F. Cabello, A. Bernardos e S. Marcelino, «A novel high-efficiency solar thermal power plant featuring electricity storage - Ideal for the future power grid with high shares of renewables,» in *SOLARPACES 2020: 26th International Conference on Concentrating Solar Power and Chemical Energy Systems*, Freiburg, 2022.

[16] «ASTERix&CAESar,» [Online]. Available: https://asterix-caesar.eu/.

[17] D. Annaratone, Steam generators description and design, Springer, 2008.

[18] S. a. S. C. Mazzoni, «Steam Cycle Simulator for CHP Plants,» *Proceedings of the ASME Turbo Expo,* vol. 2, 2013.

[19] V. Ganapathy, Industrial boilers and heat steam generators, design applications and calculations, New York: Marcel DekerInc, 2002.

[20] A. Rezaie, G. Tsatsaronis e U. Hellwig, «Thermal design and optimization of a heat recovery steam generator in a combined-cycle power plant by applying a genetic algorithm,» *Energy,* vol. 168, pp. 346-357, 2019.

[21] D. Aquaro e M. Pieve, «High temperature heat exchangers for power plants: Performance of advanced metallic recuperators,» *Applied Thermal Engineering,* vol. 27, pp. 389-400, 2007.

[22] J. Baigorri, A. Federici, T. Kubikova, T. Du Toit, P. Rodriguez-deArriba, C. Salvini, D. Sanchez e F. Zaversky, «Modelling of an Innovative Integration of Compressed Air Energy Storage (CAES) with High-Temperature oncentrated Solar Power (CSP): a Comprehensive Use-Case Study,» *Journal of Energy Storage,* 2025 (in press).